Investigation of Parameters of Band-Pass Filters on Conductivity of p-Si and p-Ge Semiconductors

V. Rusen[a], A. Katkevičius[a],
S. Tolvaišienė[b] and D. Plonis [a,*]

[a] *Vilnius Gediminas Technical University, Department of Electronic Systems, Naugarduko Str. 41-413, LT-03227, Vilnius, Lithuania*
[b] *Vilnius Gediminas Technical University, Department of Electrical Engineering, Naugarduko Str. 41-318, LT-03227, Vilnius, Lithuania*

Received: 23.05.2021 & Accepted: 29.07.2021

Doi: 10.12693/APhysPolA.140.122 *e-mail: darius.plonis@vilniustech.lt

Wireless communication technologies, including 5G and others, require devices with a reconfigurable frequency range. Frequency selection is performed with the use of various band-pass filters. Structures of the microstrip band-pass filters are popular due to their small dimensions and a convenient procedure of manufacture. We have calculated design parameters of parallel-coupled half-wave band-pass filter by using transmission line theory. The obtained design parameters have been verified with Sonnet® and CST Microwave Studio® software packages. We have chosen p-Si and p-Ge semiconductor substrates for the band-pass filter. The obtained 3.162–3.971 GHz passband is suitable for the 5G applications. The investigation has also showed that the electrical conductivity of the substrate has impact on the S-parameters of the band-pass filter. The passband of the band-pass filter becomes narrower with the increase of the electrical conductivity of the substrate.

topics: microwaves, 5G, filters, microstrip

1. Introduction

The latest trending technology in the wireless communications field is 5G. The technology is expected to provide and support faster low latency broadband communication and massive machine communication, as well to increase the full potential of technologies of the Internet of Things. The sub-6 GHz spectrum offers good coverage and capacity and it is expected to be used for 5G communication together with mm-wave band (24.25–52.6 GHz) [1]. The focus is based on bands in the range of 3.3–3.8 GHz and above 24 GHz (the range 26 GHz and 28 GHz is the 5G higher range). The range of 3.3–3.8 GHz might be the basis for many initial 5G services [2] and the demand for devices that allow communication in this range will increase.

Reconfigurability or tunability is the essential parameter in modern communication technologies. Reconfigurable filters enable more efficient handling of multiple tasks and reduce the number of additional components, which are needed in the communication systems. Electronically tunable devices allow to reduce the size and cost of the system, therefore the demand for such devices and technologies is high [3–5].

There are several methods to achieve tunability. Discrete tunability can be described as a method, where a change in parameters is achieved by using switching devices, such as PIN diodes, FET transistors, or MEMS elements [6]. The other method for achieving tunability is the selection of materials that can change parameters based on external impact. A good example of this method is graphene. The conductivity of graphene can be changed by applying different electric fields [7]. The most common approach is to use graphene instead of metal in the technologies of filter and antenna devices. This allows to tune the conductivity of the metal and achieve the required parameters.

Semiconductor materials are also interesting from the tunability perspective. Semiconductor materials are very temperature-dependent materials and their properties mostly depend on two parameters: temperature and density of impurities that influence the mobility of a semiconductor and have a direct effect on the conductivity of the material [8]. Semiconductor materials are discussed as a substrate in cases when compatibility with standard manufacturing technologies for the microwave devices is required. Typically, high-resistivity silicon with constant conductivity values is used as a substrate in filter design [9, 10]. However, parameters of semiconductors, such as electrical resistivity, impact the parameters of microwave devices built on this substrate. Different n-channel MOSFET photoresponse data were reported with substrate which was made from low resistivity silicon (with local 40 μm membranes) and with a substrate which was made from high resistivity silicon (thinned by grinding) in [11]. In some cases, adding a silicon substrate to a structure can be considered as an additional mean of tunability. Different values of dispersion characteristics depending on the material profile and semiconductor concentration are demonstrated for a graded index material on semiconductors substrate that allows to vary the frequency range of the surface wave [12].

In this study, the conventional parallel-coupled half-wave microstrip band-pass filter (BPF) is adapted to operate in the 5G frequency band. The central passband frequency f_0 of the BPF is synthesized to be equal to 3.6 GHz. The conventional dielectric substrate of the BPF was replaced with a tunable p-Si or p-Ge semiconductor substrate in order to design the reconfigurable BPF. The performance of BPF is investigated based on the analysis of S-parameters. The influence of the electrical conductivity of the semiconductor substrate on S-parameters is discussed in detail.

2. Materials and method

The electrical conductivity of semiconductors σ depends on carrier mobility μ_e and carrier density N, and can be expressed as $\sigma = eN\mu_e$, where e is the fundamental unit of electric charge [13]. The mobility of the carrier depends on temperature and on a doping level (carrier density). Values of conductivity σ for different densities of the carrier can be extracted from the mobility dependencies curves. For this purpose, the dependencies of hole mobility on doping values are used in order to extract the mobility values for selected densities to calculate the p-Si and p-Ge conductivities' values [14, 15].

The structure of a parallel coupled half wave resonator microstrip BPF is often used for filtering in microwave bands, and was therefore selected for the experiment. The structure is conventional and is presented in detail in [16, 17]. The adjacent resonators are positioned in parallel to each other and shifted by half of their length (see Fig. 1). According to [18, 19], this type of construction gives a relatively large coupling for a given spacing between resonators.

Design equations for the parallel coupled half wave resonator microstrip BPF are [19]:

$$\frac{J_{01}}{Y_0} = \sqrt{\frac{\pi}{2}\frac{\text{FBW}}{g_0 g_1}}, \tag{1}$$

$$\frac{J_{j,j+1}}{Y_0} = \frac{\pi}{2}\frac{\text{FBW}}{\sqrt{g_j g_{j+1}}}, \quad \text{for } j = 1, \dots, n-1 \tag{2}$$

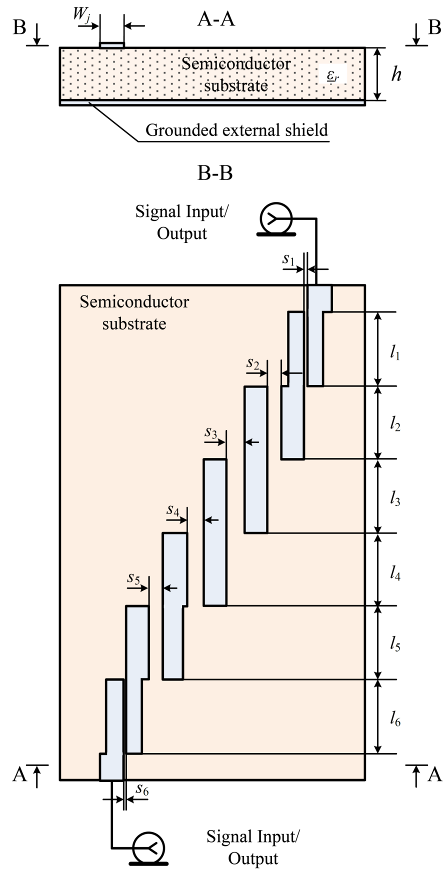

Fig. 1. Design parameters of model of BPF on a semiconductor substrate, where w_j is the width of a separated resonator, l_j is the length of a separated resonator, s_j is the gap between adjutant resonators ($j = 1, 2, \dots, 6$), and ε_r is the complex permittivity of a semiconductor substrate.

$$\frac{J_{n,n+1}}{Y_0} = \sqrt{\frac{\pi}{2}\frac{\text{FBW}}{g_n g_{n+1}}}, \tag{3}$$

where $J_{j,j+1}$ are the characteristic admittances of the admittance inverters (J-inverters), Y_0 is the characteristic admittance of the terminating lines, FBW — fractional bandwidth of filter, and g_0, $g_1, \dots,$ g_n are the ladder type lowpass prototypes with normalized cut-off $\Omega_c = 1$.

We apply (1)–(3) to calculate constants of impedance inverter for all filter line pairs, since the characteristic admittances are inversely proportional to characteristic impedances of the microstrip line.

Having J-inverters calculated, the even and odd modes of characteristic impedances can be determined for a given $j = 0, \dots, n$ using [18, 19]:

$$(Z_{0e})_{j,j+1} = \frac{1}{Y_0}\left[1 + \frac{J_{j,j+1}}{Y_0} + \left(\frac{J_{j,j+1}}{Y_0}\right)^2\right], \tag{4}$$

$$(Z_{0o})_{j,j+1} = \frac{1}{Y_0}\left[1 - \frac{J_{j,j+1}}{Y_0} + \left(\frac{J_{j,j+1}}{Y_0}\right)^2\right]. \tag{5}$$

Now, $1/Y_0$ equals Z_0 which means the characteristic impedance of the system — equal to 50 Ω for our system.

To proceed with filter design, it is necessary to find dimensions of coupled microstrip lines that gives the desired impedances of even and odd modes. The mathematical model, which was presented in [17, 20], allows to calculate the even and odd modes impedances. The calculations are based on the determination of the shape ratios of the equivalent single resonators of a microstrip line [21].

Characteristic impedances for a single microstrip line are as follows [17, 21]:

$$Z_{0so} = \frac{(Z_{0o})_{j,j+1}}{2}, \tag{6}$$

$$Z_{0se} = \frac{(Z_{0e})_{j,j+1}}{2}. \tag{7}$$

The approximate expressions for single microstrips allow to calculate their ratios of the width W and height h, hence for this the Wheeler [18, 22] and Hammerstad [19, 23] equations are used. For $W/h \le 2$:

$$\frac{W}{h} = \frac{8\exp(A)}{\exp(2A-2)}, \tag{8}$$

where

$$A = \frac{Z_c}{60}\left(\frac{\varepsilon_r+1}{2}\right)^{\frac{1}{2}} + \frac{\varepsilon_r-1}{\varepsilon_r+1}\left(0.23+\frac{0.11}{\varepsilon_r}\right). \tag{9}$$

For $W/h > 2$:

$$\frac{W}{h} = \frac{2}{\pi}\Big[(B-1) - \ln(2B-1)\Big] + \frac{2}{\pi}\frac{\varepsilon_r-1}{2\varepsilon_r}\left[\ln(B-1)+0.39-\frac{0.61}{\varepsilon_r}\right], \tag{10}$$

where

$$B = \frac{60\pi^2}{Z_C\sqrt{\varepsilon_r}}. \tag{11}$$

Using the above equations, the width and height ratios for a single microstrip line for even and odd modes can be calculated. Characteristic impedance values of the single microstrip line in (6) and (7) are equivalent to the use of Z_C in (8)–(11). Once the width and height ratios of even and odd modes are determined in the case of the single microstrip line, now the ratios W/h and s/h for the coupled microstrip line can also be calculated [21]:

The expressions for the width of microstrip lines W and the gap (spacing) s for each pair are the following:

$$\frac{s}{h} = \frac{2}{\pi}\cosh^{-1}\left(\frac{\cosh\left(\frac{\pi}{2}\left(\frac{W}{h}\right)_{se}\right) + \cosh\left(\frac{\pi}{2}\left(\frac{W}{h}\right)_{so}\right) - 2}{\cosh\left(\frac{\pi}{2}\left(\frac{W}{h}\right)_{so}\right) - \cosh\left(\frac{\pi}{2}\left(\frac{W}{h}\right)_{se}\right)}\right), \tag{12}$$

$$\frac{W}{h} = \frac{1}{\pi}\left[\cosh^{-1}\left(\frac{1}{2}\left(\cosh\left(\frac{\pi s}{2h}\right) - 1 + \left(\cosh\left(\frac{\pi s}{2h}\right)+1\right)\cosh\left(\frac{\pi}{2}\left(\frac{W}{h}\right)_{se}\right)\right)\right) - \frac{\pi s}{2h}\right]. \tag{13}$$

The effective dielectric constant for each microstrip is calculated using [19, 21]:

$$\varepsilon_{\text{eff}} = \frac{\varepsilon_r+1}{2} + \frac{\varepsilon_r-1}{2}\frac{1}{\sqrt{1+\frac{12h}{w}}}. \tag{14}$$

Knowing (14), the guided wavelength of a quasi-TEM mode of microstrip can be computed [19, 21]. Namely,

$$\lambda_g = \frac{\lambda_0}{\sqrt{\varepsilon_{\text{eff}}}}, \tag{15}$$

where λ_0 is the wavelength of free space. The length of each resonator is [19, 21]:

$$l = \frac{\lambda_g}{4} = \frac{c}{4f\sqrt{\varepsilon_{re}}}. \tag{16}$$

The design parameters of parallel coupled half wave resonator microstrip BPF for the 5G applications are calculated according to the conventional methods, which are discussed in the paragraph above [17, 19–21]. The filter is designed for $f_{c1} = 3.4$ GHz and $f_{c2} = 3.8$ GHz, the lower and higher cutoff frequencies, respectively. The fractional bandwidth (FBW) of the designed BPF equals 0.111. The 5th order Chebyshev filter with 0.1 dB ripples is used in the design parameters determination procedure. The thickness $h = 0.635$ mm is used for both p-Si ($\varepsilon_r = 11.7$) and p-Ge ($\varepsilon_r = 16.2$) semiconductor substrates of the BPF. Other design parameters values like W_j — the width of a separated resonator, l_j — the length of separated resonator and s_j — the gap between adjutant resonators are presented in (Table I). The design parameters vary for the different substrates because the dielectric permittivity of different semiconductors is different. This, in fact, influences the parameters of the filter itself.

TABLE I

Physical parameters of BPF with $f_0 = 3.6$ GHz central frequency for 5G applications on the p-Si and p-Ge substrates.

j	Si ($\varepsilon_r = 11.7$)			Ge ($\varepsilon_r = 16.2$)		
	W_j	s_j	l_j	W_j	s_j	l_j
1, 6	0.392	0.089	7.590	0.271	0.116	6.585
2, 5	0.559	0.355	7.484	0.394	0.407	6.496
3, 4	0.573	0.452	7.476	0.404	0.507	6.490

The structure of the band-pass filter is symmetrical (see Fig. 1). The overall 50.61 mm length and 20 mm width are selected for the p-Ge substrate, while the 45.54 mm length and 20 mm width are selected for the p-Si substrate. Two different p-Si and p-Ge semiconductors are used for the substrate due to their different conductivity. Semiconductors have a specific property to vary the mobility of carriers when the density of carriers is changing. The dimensions of separated resonators vary and depend on the position in the band-pass filter (Table I). The thickness of the conductor is equal to 0.035 mm in all cases.

The impact of conductivity on the S-parameters of the band-pass filter is evaluated with computer models in Sonnet® and CST Microwave Studio® software packages.

3. Results and discussion

The design parameters (Table I) of the BPF are calculated using the transmission line theory and they are aimed to work specifically in the 5G frequency bands. Models of BPFs are verified in Sonnet® and CST Microwave Studio® software packages. The collected S-parameters provide data for the analysis and discussion. We have shown the dependence of S-parameters on the conductivity for a constant temperature, where p-Si and p-Ge semiconductor materials are used for the substrate.

3.1. Impact of semiconductor on S-parameters

The calculated design parameters are applied to the model of band-pass filter with both p-Si and p-Ge semiconductor substrates. The models of BPFs are designed in the Sonnet® software package.

First of all, the basic model of the band-pass filter is performed and analyzed without taking the conductivity parameter into account ($\sigma = 0$ S/m). The results show that (i) the lower cutoff frequency of the band-pass filter is equal to $f_{c1} = 3.162$ GHz, and (ii) the higher cutoff frequency is equal to $f_{c2} = 3.909$ GHz. These results are obtained with the p-Si semiconductor substrate. The width of the passband is $\Delta f = 0.747$ GHz, which is almost twice as wide as the desirable passband, 0.4 GHz, stated in the 5G specification (see Table II). It is also important to mention that both the low f_{c_1} and high f_{c_2} cutoff frequencies are also shifted away from the central frequency. Note that the central frequency is shifted towards lower frequencies by 0.1 GHz (see Fig. 2).

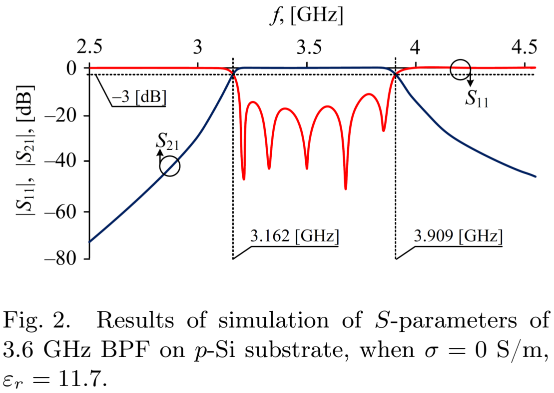

Fig. 2. Results of simulation of S-parameters of 3.6 GHz BPF on p-Si substrate, when $\sigma = 0$ S/m, $\varepsilon_r = 11.7$.

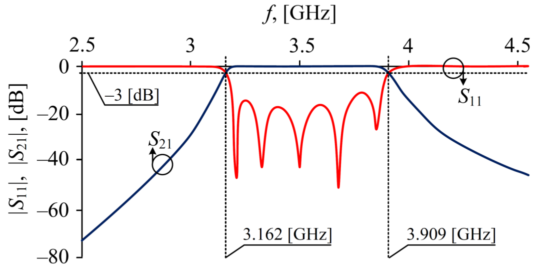

Fig. 3. Results of simulation of S-parameters of 3.6 GHz BPF on a p-Ge substrate, when $\sigma = 0$ S/m, $\varepsilon_r = 16.2$.

TABLE II

Comparison of passband on −3 dB level of BPFs models on Si and Ge substrates and $\sigma = 0$ S/m with preferable passband from 5G specification.

	f_{c_1} [GHz]	f_{c_2} [GHz]	f_c [GHz]	Δf [GHz]
frequency	3.4	3.8	3.6	0.4
filter on Si substrate	3.162	3.909	3.5	0.747
filter on Ge substrate	3.177	3.869	3.5	0.692

Analogous results of the model of the band-pass filter on p-Ge substrate show that the lower and higher cutoff frequencies are equal to $f_{c1} = 3.177$ GHz and $f_{c2} = 3.869$ GHz, respectively (see Fig. 3).

The width of the passband is equal to 0.692 GHz. The obtained central frequency is equal to 3.5 GHz. One can see that the obtained passband is 73% wider in comparison with the preferable width of the passband according to the 5G specification (see Table II).

The passband of the filter on the p-Ge substrate is narrower (0.692 GHz) as compared to the passband (0.747 GHz) of the filter on the p-Si semiconductor. However, the difference is insignificant, i.e., it is only 55 MHz.

3.2. Impact of carrier density on S-parameters

The S-parameters are obtained for BPFs on p-Si and p-Ge substrates with different carrier densities values N that lead to a change in the material's conductivity. The temperature is set to $T = 300$ K. Based on the p-Si hole mobility dependence on carrier density in 300 K, the electrical conductivity values are calculated for $N = N_a = 5 \times 10^{15}$, 10^{16}, 5×10^{16}, 10^{17}, 5×10^{17} cm^{-3} (where N_a is the acceptor density). The higher carrier density results are obtained when the higher electrical conductivity

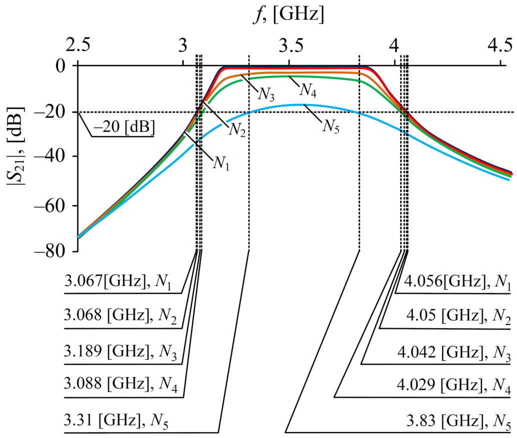

Fig. 4. The S_{21}-parameters of BPF on the p-Si substrate for temperature T = const and when carrier density is: $N_1 = 5 \times 10^{15}$ cm^{-3}, $N_2 = 10^{16}$ cm^{-3}, $N_3 = 5 \times 10^{16}$ cm^{-3}, $N_4 = 10^{17}$ cm^{-3}, and $N_5 = 5 \times 10^{17}$ cm^{-3}.

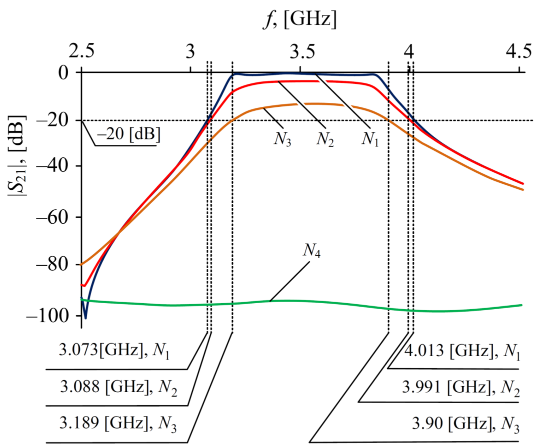

Fig. 5. The S_{21}-parameters of BPF on the p-Ge substrate for temperature T = const and when carrier density is: $N_1 = 3.2 \times 10^{15}$ cm^{-3}, $N_2 = 2.7 \times 10^{16}$ cm^{-3}, $N_3 = 1.2 \times 10^{17}$ cm^{-3}, and $N_4 = 4.9 \times 10^{18}$ cm^{-3}.

of the substrate is used at constant temperature. The curves of S_{21} parameter of the band-pass filter, which is located on the p-Si semiconductor substrate, are presented in Fig. 4.

In Fig. 4, one can see the increase of loss on the increase of density which is caused by the increase of the conductivity of the material. The acceptor density $N = N_a = 5 \times 10^{17}$ cm^{-3} gives the highest attenuation.

The conductivity values for the band-pass filter on the p-Ge semiconductor substrate are obtained by estimating different $N = N_a - N_d$ values (where N_d is the donor density). The conductivity values are calculated for $N = 3.2 \times 10^{15}$, 2.7×10^{16}, 1.2×10^{17}, 4.9×10^{18} cm^{-3}. The same pattern with increasing losses on increased density can be obtained from the S_{21} parameters (Fig. 5).

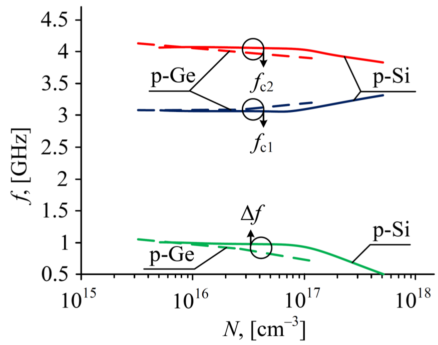

Fig. 6. Analysis of the bandwidth of BPFs on the p-Si and p-Ge substrates.

The passband of the band-pass filter depends on the conductivity of the substrate. The passband is wider when the p-Si semiconductor is used for the substrate. The analysis of S-parameters shows that the passband tends to shrink when the carrier density of the substrate is increasing (Fig. 6). The measurements are taken in the vicinity of -20 dB.

3.3. Analysis of complex permittivity of BPF

Firstly, the analysis of complex permittivity of BPF is performed by using the plasma resonance frequency of the substrate of BPF and by taking into account the semiconductor lattice permittivity $\varepsilon_L = \varepsilon_r \varepsilon_0$, where $\varepsilon_0 = 10^{-9}/(36\pi)$ F/m. The plasma resonance frequency $f_p(N)$ of the substrate of BPF can be calculated selecting different values of carrier densities N of the p-Ge and p-Si semiconductors. Then, one relies on the following relation:

$$f_p(N) = \frac{q^2 N}{2\pi m^* \varepsilon_L}, \tag{17}$$

where q is the charge of the holes $(1.60217733(49) \times 10^{-19}$ C$)$, $m^* = m_k m_e$ is the effective mass of holes in the semiconductor, m_k is the mass of holes and m_e is the mass of the electron.

The effective heavy hole masses of the p-Si semiconductor are $m_1^* = 0.49 m_e$ and the light hole masses $m_2^* = 0.16 m_e$. The effective heavy hole masses of the p-Ge semiconductor are $m_1^* = 0.33 m_e$ and the light hole masses are $m_1^* = 0.043 m_e$.

Secondly, the central working frequency of the band-pass filter is selected for the analysis of complex permittivity of this band-pass filter. The central working frequency of the band-pass filter could be calculated by using the equation

$$f_0 = f_{c1} + \frac{f_{c2} - f_{c1}}{2}. \tag{18}$$

The complex permittivity at central working frequency (and plasma resonance frequency) of the band-pass filter could be calculated by using equation

$$\varepsilon_r^s(N, \omega) = \varepsilon_L \left(1 - \frac{j\omega_p(N)}{\omega} \frac{1}{\zeta + j\omega}\right), \tag{19}$$

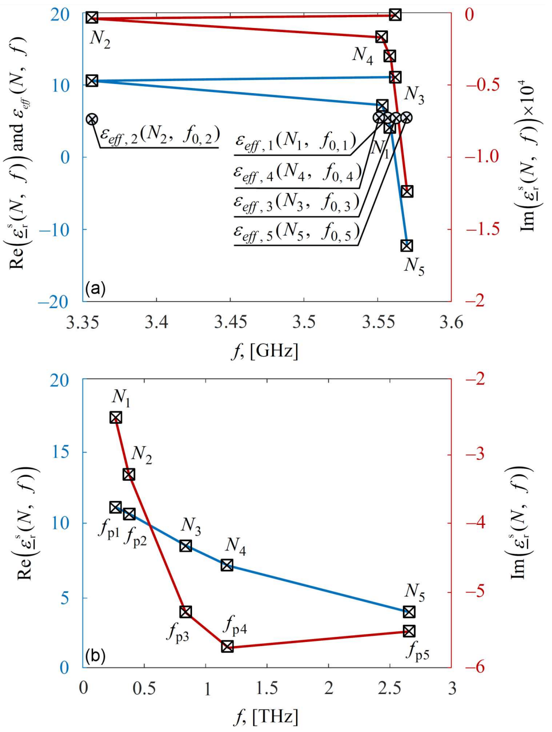

Fig. 7. Analysis of the complex permittivity of the p-Si BPF: (a) complex permittivity in GHz range, (b) – complex permittivity in THz range, when $N_1 = 5 \times 10^{15}$ cm^{-3}, $N_2 = 10^{16}$ cm^{-3}, $N_3 = 5 \times 10^{16}$ cm^{-3}, $N_4 = 10^{17}$ cm^{-3}, and $N_5 = 5 \times 10^{17}$ cm^{-3}.

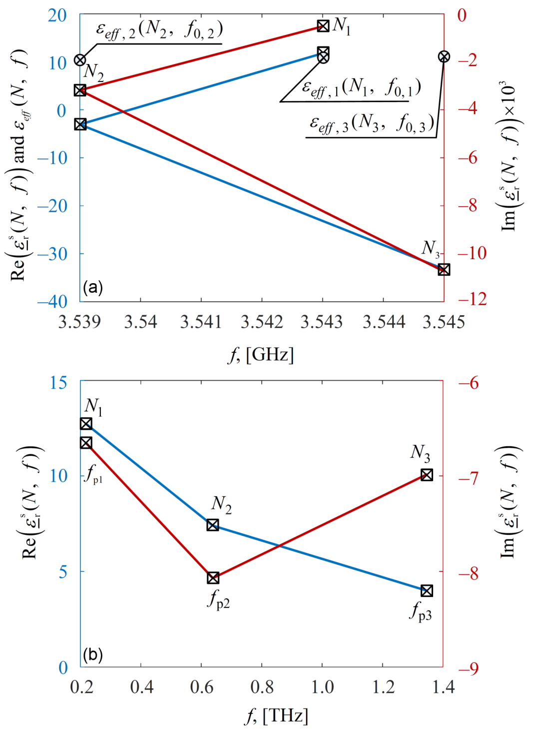

Fig. 8. Analysis of the complex permittivity of the p-Ge BPF: (a) complex permittivity in GHz range, (b) complex permittivity in THz range, when $N_1 = 3.2 \times 10^{15}$ cm^{-3}, $N_2 = 2.7 \times 10^{16}$ cm^{-3}, and $N_3 = 1.2 \times 10^{17}$ cm^{-3}.

where $\xi = q/(\mu m^*)$ is the collision frequency of the free carrier, $\omega_p(N) = 2\pi f_p(N)$ is the angular plasma resonance frequency and $\omega = 2\pi f$ is the angular operating frequency.

The operating frequency f will be changed with the central working frequency of the BPF f_0 and the plasma resonance frequency f_p in the analysis of the complex permittivity of the BPF.

The analysis of the complex permittivity of the p-Si BPF (Fig. 7) is performed for the selected values of the density of holes: $N = 5 \times 10^{15}$, 10^{16}, 5×10^{16}, 10^{17}, 5×10^{17} cm^{-3} at 300 K. In addition, the effective permittivity $\varepsilon_{\mathrm{eff}}(N, f)$ of the BPF was calculated in the framework of the complex permittivity study.

It should be emphasized that the real part of the complex permittivity $\mathrm{Re}(\underline{\varepsilon}_r^s(N,\omega))$ of the p-Si BPF decreases when the density of the holes increases typically from 5×10^{15} cm^{-3} up to 5×10^{17} cm^{-3}. The central working frequency f_0 of the BPF moves then from $f_{01} = 3.562$ GHz to $f_{05} = 3.57$ GHz (Fig. 7a). In turn, the imaginary part of the complex permittivity $\mathrm{Im}(\underline{\varepsilon}_r^s(N,\omega))$ of the p-Si BPF increases when the density of the holes increases. The lowest value of $\mathrm{Im}(\underline{\varepsilon}_r^s(N,\omega))$ could be received when the density of holes is equal to $N_3 = 5 \times 10^{16}$ cm^{-3}. The highest $\mathrm{Im}(\underline{\varepsilon}_r^s(N,\omega))$ could be received when the density of holes is equal to $N_5 = 5 \times 10^{17}$ cm^{-3}. This could be explained by the fact that the complex permittivity depends on the density of holes and collision frequency of the free carrier, which depends on the mobility μ of the carrier. Moreover, a very high imaginary part of the complex permittivity of the p-Si BPF $\mathrm{Im}(\underline{\varepsilon}_r^s(N,\omega))$ shows that the electromagnetic attenuation of the electromagnetic waves is very high in the p-Si BPF and it means that filters should be manufactured with the lower density of the holes N at 300 K.

The effective permittivity $\varepsilon_{\mathrm{eff}}(N,\omega)$ of the p-Si BPF increases when the density of the holes N at 300 K increases. The effective permittivity of the p-Si BPF increases in all width of the passband Δf of the p-Si BPF at different densities of the holes.

The analysis of the plasma resonance frequency f_p will not have any effect on the scattering characteristics of the p-Si BPF (Fig. 7b). The analysis shows that $\mathrm{Im}(\underline{\varepsilon}_r^s(N,\omega))$ of the p-Si BPF is lower in the THz frequency range than in the GHz frequency range. The plasma resonance frequency f_p increases, when N increases. The lowest plasma resonance frequency f_{p1} is received, when the density of the holes is $N_1 = 5 \times 10^{15}$ cm^{-3} and the highest f_{p5}, when the density is equal to $N_5 = 5 \times 10^{17}$ cm^{-3}.

The results of the analysis of the complex permittivity of the p-Ge BPF are presented in Fig. 8, where the density of the carrier is equal to: $N = 3.2 \times 10^{15}$, 2.7×10^{16}, 1.2×10^{17} cm^{-3} at 300 K. The real part of complex permittivity of the p-Ge BPF decreases, when the density of the holes increases from 3.2×10^{15} cm^{-3} up to 2.7×10^{16} cm^{-3}. The central working frequency f_0 of the BPF moves then from $f_{0,1} = 3.562$ GHz to $f_{0,2} = 3.39$ GHz and finally increases up to $f_{0,3} = 3.545$ GHz (Fig. 8a). The highest imaginary part of the complex permittivity of the p-Ge BPF could be received, when the density of holes is $N_3 = 1.2 \times 10^{17}$ cm^{-3}.

The effective permittivity $\varepsilon_{\text{eff}}(N, \omega)$ of the p-Ge BPF is almost the same in all investigated frequencies. Namely, $\varepsilon_{\text{eff}}(N, \omega) \cong \text{Re}\,(\underline{\varepsilon}_r^s(N, \omega)) \cong 10.74$, assuming the density of the holes to be $N_1 = 3.2 \times 10^{15}$ cm^{-3}.

The analysis has showed that the plasma resonance frequency f_p will not have any effect on the scattering characteristics of the p-Ge BPF (Fig. 8b). The analysis has also showed that the real part of the complex permittivity $\text{Re}(\underline{\varepsilon}_r^s(N, \omega))$ of the p-Ge BPF decreases with increase of frequency in the THz frequency range. The lowest value of the imaginary part of the complex permittivity of the p-Ge BPF is obtained when the density of holes is equal to $N_2 = 2.7 \times 10^{16}$ cm^{-3} at the $f_{p2} = 0.6258$ THz plasma resonance frequency.

3.4. Comparison of results

The results of S_{11} and S_{21} parameters are obtained with the method of moments (MoM) in the Sonnet® software package. These results are compared with the results obtained with the finite-difference time-domain method (FDTD) in CST Microwave Studio®. The continuous lines represent the results from Sonnet® and the dotted lines represent those from CST Microwave Studio®. The blue curve shows the variation of S_{11} while the red curves represent the variation of S_{21} (Fig. 9a and b).

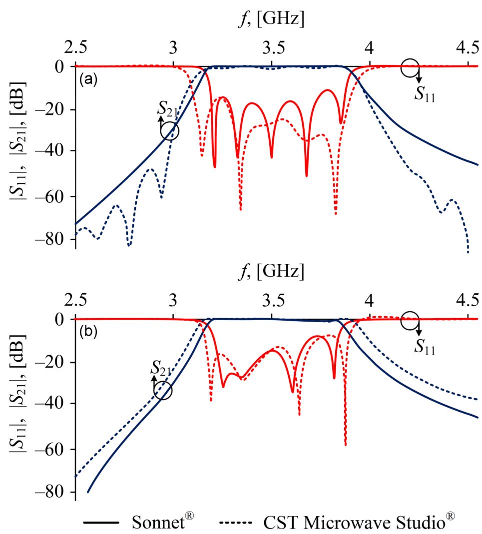

Fig. 9. Comparison of S_{11} and S_{21} parameters of BPFs with (a) the p-Si substrate and (b) the p-Ge substrate using the MoM or FDTD methods.

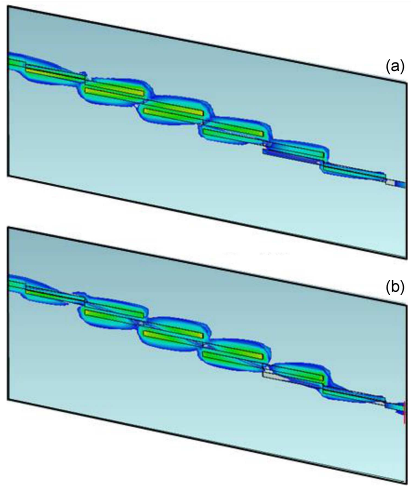

Fig. 10. The E-field of BPF with the p-Si substrate, at (a) 3.162 GHz and (b) 3.909 GHz cutoff frequencies.

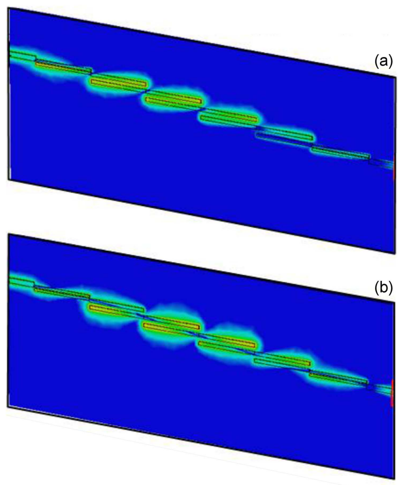

Fig. 11. The E-field of BPF with the p-Ge substrate, at (a) 3.177 GHz and (b) 3.869 GHz cutoff frequencies.

The results of the model of BPF on the p-Si substrate ($\varepsilon_r = 11.7$) are presented in Fig. 9a, while the results of the model of BPF on p-Ge substrate ($\varepsilon_r = 16.2$) are presented in Fig. 9b. All design parameters in CST Microwave Studio® are kept the same as in Sonnet®. All dimensions of design parameters are given in Table I. The analysis is performed by comparing the parameters of reflection coefficient S_{11} and transmission coefficient S_{21}.

The low cutoff frequency 3.145 GHz and the high cutoff frequency 3.971 GHz are obtained with the FDTD method in CST Microwave Studio® when the p-Si semiconductor is used for the substrate. Slightly different $f_{c1} = 3.162$ GHz and $f_{c2} = 3.909$ GHz cutoff frequencies are obtained in Sonnet® with the method of moments (Fig. 9a). The low cutoff frequency $f_{c1} = 3.195$ GHz and the high cutoff frequency $f_{c2} = 3.967$ GHz are obtained in CST Microwave Studio® when the p-Ge semiconductor is used for the substrate and, in comparison, the $f_{c1} = 3.177$ GHz and $f_{c2} = 3.869$ GHz cutoff frequencies are obtained in Sonnet® (Fig. 9b). The low cutoff frequency f_{c1}, which is obtained with the different methods in different construction, varies no more than 50 MHz. The high cutoff frequency f_{c2} varies no more than 40 MHz. The average width of the passband is equal to 760 MHz. The variations of the width of the passband do not exceed 80 MHz with different methods.

The distribution of E-field at the cutoff frequencies $f_{c1} = 3.162$ GHz and $f_{c2} = 3.909$ GHz observed in individual filter elements is presented in Fig. 10a and b. The p-Si semiconductor is used for the substrate.

The distribution of E-field at the cutoff frequencies $f_{c1} = 3.177$ GHz and $f_{c2} = 3.869$ GHz observed in individual filter elements is presented in Fig. 11a and b. The p-Ge semiconductor is used for the substrate.

4. Conclusions

The attenuation of the electromagnetic waves depends on the complex permittivity of the substrate in BPFs. The highest attenuation of the electromagnetic waves can be received in BPFs with the p-Si substrate. The highest attenuation of the electromagnetic waves is received, when the density of acceptor impurities is $N = N_a = 5 \times 10^{17}$ cm^{-3}.

The passband of BPFs depends on the resistivity (or conductivity) of substrate. The widest passband can be received in p-Si BPFs. In the case of the passband of 1 GHz, it can be received in the range of carrier densities equal to 5×10^{15}–5×10^{17} cm^{-3}.

The passband of p-Ge BPF is narrower than the passband of p-Si BPF because these materials have different permittivities. However, the attenuation of the electromagnetic waves is lower in the p-Ge BPFs at high densities of impurities.

The analysis of complex permittivity of the BPF is performed in detail, by using plasma resonance frequency of the substrate and by taking into account the semiconductor lattice permittivity. The complex permittivity depends on the density of the holes and the central working frequency of the BPF. The real part of the complex permittivity decreases with the increase of the density of the holes. The imaginary part of the complex permittivity increases with the increase of the density of the holes.

Notably, the results, which are obtained by different MoM and FDTD methods, corresponds to each other. The difference of f_{c_1} does not exceed 50 MHz. The difference of f_{c_2} is smaller than 40 MHz. The passband varies no more than 80 MHz with different methods. The average passband is equal to 760 MHz.

Future work considerations include replacing copper with graphene and replacing the semiconductor substrate with a liquid crystal substrate. The S-parameters could be predicted by using artificial neural networks.

References

[1] Wei Hong, Zhi Hao Jiang, Chao Yu, Debin Hou, Haiming Wang, Chong Guo, Yun Hu, Le Kuai, Yinrui Yu, *IEEE J. Microwaves* **1**, 101 (2021).

[2] GSMA, 5G Spectrum, Public Policy Position, 2019.

[3] Y. Tu, Y.I.A. Al-Yasir, N.O. Parchin, A.M. Abdulkhaleq, R.A. Abd-Alhameed, *Electronics* **9**, 1 (2020).

[4] Y.I.A. Al-Yasir, N.O. Parchin, R.A. Abd-Alhameed, A.M. Abdulkhaleq, J.M. Noras, *Electronics* **8**, 114 (2019).

[5] Xiaoguang Liu, in: *Proc. 2015 IEEE 16th Annu. Wirel. Microw. Technol. Conf. WAMICON 2015*, Vol. C, 2015, p. 15.

[6] R. Allanic, D. Le Berre, Y. Quéré, C. Quendo, D. Chouteau, V. Grimal, D. Valente, J. Billoué, in: *2018 IEEE 22nd Workshop on Signal and Power Integrity (SPI)*, Vol. C, 2018, p. 17895917.

[7] V. Slegeryte, D. Belova-Ploniene, A. Katkevicius, D. Plonis, in: *Proc. 2019 IEEE Microw. Theory Tech. Wirel. Commun. MTTW 2019*, Vol. 1, 2019, p. 87.

[8] R. Allanic, D. Le Berre, C. Quendo, D. Chouteau, V. Grimal, D. Valente, J. Billoué, *Electronics* **9**, 1 (2021).

[9] L. Wu, J. Mao, F. Hou, J. Zhu, in: *2017 IEEE Electrical Design of Advanced Packaging and Systems Symposium (EDAPS), Haining (China)*, 2017, p. 1.

[10] T. Chen, W. Hu, P. Sun, K. Zhang, in: *Proc. 2020 21st Int. Conf. on Electronic Packaging Technology (ICEPT), Guangzhou (China)*, 2020, p. 1.

[11] K. Kucharski, P. Zagrajek, D. Tomaszewski, A. Panas, G. Głuszko, J. Marczewski, P. Kopyt, *Acta Phys. Pol. A* **130**, 1193 (2016).

[12] T. Gric, *Acta Phys. Pol. A* **129**, 352 (2016).

[13] S. Kasap, P. Capper, *Springer Handbook of Electronic and Photonic Materials*, Springer, 2017, p. 1536.

[14] J.M. Dorkel, P. Leturcq, *Solid State Electron.* **24**, 821 (1981).

[15] O.A. Golikova, B.Y. Moizhes, L.S. Stilbans, *Sov. Phys. Solid State* **3**, 2259 (1962).

[16] S. Girraj, D. Rajeswar, *Electronics* **1**, 1 (2013).

[17] B. Maity, I. Pradhan, in: *2015 Int. Conf. on Communications and Signal Processing (ICCSP), Melmaruvathur (India)*, 2015, p. 0950.

[18] D.M. Pozar, *Microwave Engineering*, 4th ed., Wiley, 2011, p. 752.

[19] J.-S. Hong, M.J. Lancaster, *Microstrip Filters for RF/Microwave Applications*, Wiley, 2001, p. 460.

[20] V.S. Kushwah, G.S. Tomar, in: *Proc. 2018 10th Int. Conf. Comput. Intell. Commun. Networks (CICN 2018)*, 2018, p. 31.

[21] A. Naghar, O. Aghzout, J. Naghar, H. Latioui, M. Essaaidi, *Int. J. Innov. Res. Comput. Commun. Eng.* **1**, 1601 (2013).

[22] H. Wheeler, *IEEE Trans. Microw. Theory Tech.* **13**, 172 (1965).

[23] E.O. Hammerstad, in: *Proc. European Microwave Conf., Hamburg (Germany)*, 1975, p. 268.